

Multiplicity dependence of hyperon and hypertriton production in Zr+Zr and Ru+Ru collisions at $\sqrt{s_{NN}} = 200$ GeV

Dongsheng Li^{1,*}

¹University of Science and Technology of China

Abstract. We present yield measurements on hyperons (Λ , $\bar{\Lambda}$ and Ξ^- , $\bar{\Xi}^+$) and hypertriton (${}^3_{\Lambda}\text{H}$, ${}^3_{\Lambda}\bar{\text{H}}$) in four different centrality classes of Zr+Zr and Ru+Ru collisions at $\sqrt{s_{NN}} = 200$ GeV. The yield ratios of Λ/π^- , Ξ^-/π^- , ${}^3_{\Lambda}\text{H}/\Lambda$ and $S_3 = ({}^3_{\Lambda}\text{H}/\Lambda)/({}^3\text{He}/p)$ are reported as a function of multiplicity, while the ratio of ${}^3_{\Lambda}\text{H}/{}^3\text{He}$ is reported as a function of p_T in each centrality. The comparisons between data and models are discussed. These results provide insights on particle production mechanisms in heavy-ion collisions.

1 Introduction

In analogy to the Big Bang theory which describes the origin and evolution of the universe, high energy heavy-ion collisions(HIC) can be called the little bang. Although they are different systems, measurements on particle production in HIC would possibly help us understand the first few minutes of the evolution of our universe.

Recently, the system size dependence of particle production in HIC has drawn a lot of attention [1–10, 15]. For hadron production, such dependence mainly reflects the properties of the hot medium. While for large nuclear clusters like hypertriton (${}^3_{\Lambda}\text{H}$), their internal structures might also leave some non-negligible fingerprints on the yields, because their nuclear size are of the same magnitude as the size of the fireball created in the collisions and may be even larger than the fireball size for some small collision systems. These studies aim to verify our understanding of particle production mechanisms in HIC.

2 Results and discussions

In system size studies, the charged-particle multiplicity within unit pseudo-rapidity ($dN_{ch}/d\eta$) is usually suggested as a measure of system size. In this work, we report the multiplicity dependence of hyperon and ${}^3_{\Lambda}\text{H}$ production in Zr+Zr and Ru+Ru collisions at $\sqrt{s_{NN}} = 200$ GeV. These short-lived particles are reconstructed with the KFPARTICLE Package [16], using the 2-body decay channels including $\Lambda \rightarrow p + \pi^-$, $\Xi^- \rightarrow \Lambda + \pi^-$, ${}^3_{\Lambda}\text{H} \rightarrow {}^3\text{He} + \pi^-$ and their charge conjugates. The daughter particle tracks including π^\pm , $p(\bar{p})$, ${}^3\text{He}({}^3\bar{\text{He}})$ are identified with energy loss $\langle dE/dx \rangle$ and momentum information measured by the Time Projection Chamber (TPC).

*e-mail: erl@mail.ustc.edu.cn

2.1 Hyperon-to-pion ratio

In Fig. 1, hyperon-to-pion ratios are shown as a function of multiplicity, where the solid markers show the results from this study, while open markers show results from other collision systems [1–5, 11, 12]. In this analysis, the feed-down contributions from weak decay have been subtracted for Λ and $\bar{\Lambda}$, while for Ξ^- and Ξ^+ such contributions are negligible. It is found that systems with similar multiplicity generally have a common scaling behavior, which means that the strangeness production mechanisms are similar despite differences of the collision energies and the beam particle species. These yield ratios show a slightly increasing trend from small to large systems and such enhancement is usually considered as a signature of QGP formation in large systems.

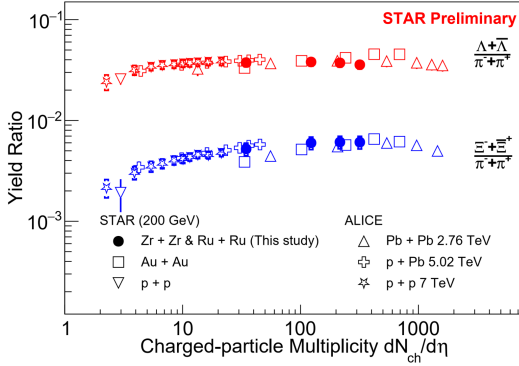


Figure 1. The hyperon-to-pion ratios as a function of charged-particle multiplicity. Yields of particles are combined with those of anti-particles. Red markers show the $(\Lambda + \bar{\Lambda})/(\pi^- + \pi^+)$ ratio, while blue markers show the $(\Xi^- + \Xi^+)/(\pi^- + \pi^+)$ ratio, respectively. The preliminary results in 200 GeV Zr+Zr and Ru+Ru collisions by this study is shown as the solid circles. Results from other collision systems are shown as open markers for comparison [1–5, 11, 12].

2.2 ${}^3_{\Lambda}\text{H}/\Lambda$ and S_3 ratios

The light hypernuclei production mechanisms in HIC are still not fully understood. The yield ratios of ${}^3_{\Lambda}\text{H}/\Lambda$ and $S_3 = ({}^3_{\Lambda}\text{H}/\Lambda)/({}^3\text{He}/p)$ are suggested as probes to distinguish different production mechanisms. Measurements on these hypernuclei yield ratios are shown in Fig. 2. In this analysis, the yields of Λ , proton and ${}^3\text{He}$ are corrected for feed-down from weak decay channels. Predictions from several popular theoretical models are also shown for comparison. The thermal model calculations are generated with canonical ensemble using the Thermal-Fist package [17]. The thermal model parameters for Zr+Zr and Ru+Ru collisions are obtained by fitting the yields of light hadrons, including π^\pm , K^\pm , p , $\Lambda(\bar{\Lambda})$ and $\Xi^-(\Xi^+)$, in each centrality. The correlation volume (V_c) is varied from $V_c = dV/dy$ to $3dV/dy$. Other thermal model parameters are varied by $1-\sigma$ to generate the uncertainty bands. The thermal model predictions for LHC energies are directly taken from [15]. The analytical coalescence model calculations are generated with several assumptions of a thermalized hadron emission source, using both 2-body and 3-body Wigner function to treat the nucleon coalescence process [18]. We also compare with another coalescence model which applies the MUSIC and UrQMD model to simulate the QGP evolution and hadronic rescattering before the coalescence. Subsequently, it uses 3-body Wigner function with different inputs of the Λ binding energy (B_Λ) of ${}^3_{\Lambda}\text{H}$ for the coalescence afterburner [19].

The S_3 ratio in this study is roughly consistent with that in Au+Au and U+U collisions [13]. The ${}^3_{\Lambda}\text{H}/\Lambda$ and S_3 ratios from this study and from the ALICE collaboration measurements [14, 15] show similar trends. These results strongly deviate from the thermal model predictions, while agreeing with calculations by coalescence model of certain configurations. In particular, we find that the MUSIC + UrQMD + Coal. model with $B_\Lambda =$

66 0.42 MeV [20] can simultaneously describe both yield ratios well. However, we note that
 67 the B_Λ averaged over all current measurements is 0.164 ± 0.043 MeV, which is significantly
 68 smaller than 0.42 MeV. An increasing trend from small to large collision systems is observed
 69 in the ${}^3_\Lambda\text{H}/\Lambda$ ratio, which is understood as a result of canonical suppression and possibly also
 70 the large nuclear size of ${}^3_\Lambda\text{H}$. While for the S_3 ratio, a much weaker multiplicity dependence
 71 is observed compared to the ${}^3_\Lambda\text{H}/\Lambda$ ratio, which is possibly due to the nuclear size effect since
 72 the conserved charges like baryon number and strangeness number all cancel out.

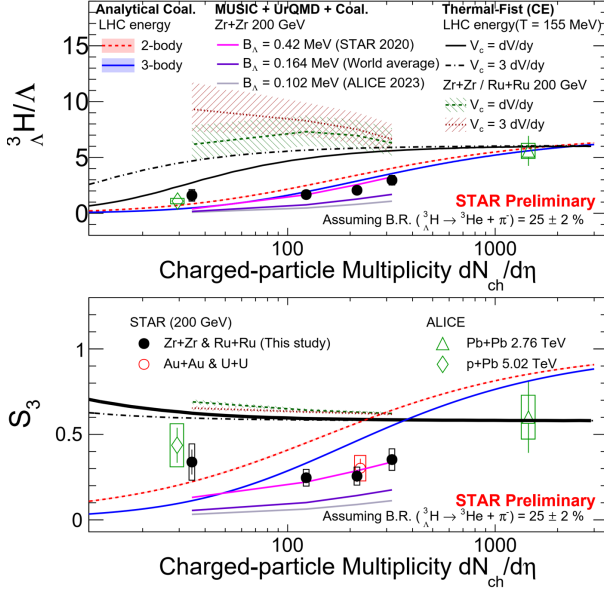


Figure 2. The multiplicity dependence of ${}^3_\Lambda\text{H}/\Lambda$ and S_3 . Solid circles show results from 200 GeV Zr+Zr and Ru+Ru collisions by this study, while open markers show results from other collision systems. Different model calculations are shown for comparison, including the analytical coalescence model (red and blue shaded bands), MUSIC + UrQMD + Coal. model of different Λ binding energy inputs (magenta, violet and grey lines) and Thermal-Fist model with the canonical ensemble assumption (black lines, green and brown shaded bands).

73 2.3 ${}^3_\Lambda\text{H}/{}^3\text{He}$ ratio

74 The constituents of ${}^3_\Lambda\text{H}$ would be the same as those of ${}^3\text{He}$ if one substitutes the Λ with a
 75 proton. Although their masses are very similar, they have very different sizes. The nuclear
 76 radius of ${}^3_\Lambda\text{H}$ is ~ 5 fm, while that of ${}^3\text{He}$ is ~ 2 fm, thus the coalescence model expects a
 77 strong multiplicity dependence and a p_T softening of the ${}^3_\Lambda\text{H}/{}^3\text{He}$ ratio [19]. While in the
 78 thermal model, all particles are treated point-like with no internal structure.

79 In Fig. 3, the ${}^3_\Lambda\text{H}/{}^3\text{He}$ ratio is measured in different centrality classes of Zr+Zr and Ru+Ru
 80 collisions, showing a weak p_T and multiplicity dependence. By comparing with the model
 81 predictions, it seems our data points are roughly described by the coalescence model with
 82 $B_\Lambda = 0.42$ MeV, while overestimated by the thermal model. Again, we note that this value
 83 seems to be too large compared with the world average value.

84 3 Summary and outlook

85 The yield measurements on hyperons (Λ , $\bar{\Lambda}$ and Ξ^- , $\bar{\Xi}^+$) and hypertriton (${}^3_\Lambda\text{H}$, ${}^3_\Lambda\bar{\text{H}}$) in Zr+Zr
 86 and Ru+Ru collisions at $\sqrt{s_{NN}} = 200$ GeV are reported in these proceedings. The multiplicity
 87 dependence of hyperon and light hypernuclei production are investigated. It is found that the
 88 hyperon production mechanisms are similar in systems with the same multiplicity, despite
 89 differences of the collision energies and the beam particle species. For light hypernuclei
 90 production, the measurements roughly agree with certain coalescence model predictions and

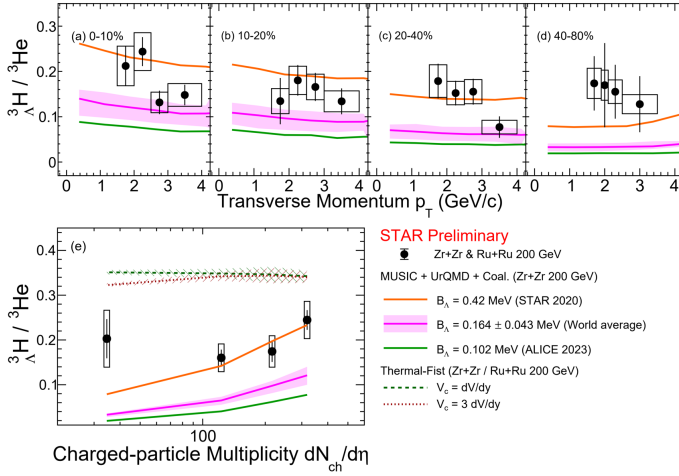


Figure 3. Fig.(a) - Fig.(d) show the p_T dependence of $^3\Lambda/\Lambda$, while Fig(e) shows the multiplicity dependence of the p_T integrated ratio. Black points show the measurement in this study. Model predictions from MUSIC + UrQMD + Coal. model of different Λ binding energy inputs are shown as orange, magenta and green lines, while Thermal-Fist are shown as the green and brown shaded bands.

91 strongly deviate from the thermal model calculations. However, the coalescence model with
 92 the world average measured B_Λ does not describe the data well. Thus, more efforts from the
 93 theoretical side, as well as higher precision measurements in small systems will be necessary
 94 to elucidate the role of the nuclear size on the formation of light hypernuclei in HIC.

95 References

- 96 [1] J. Adams et. al. (STAR collaboration), Phys. Rev. Lett. **98** (2007), 062301
 97 [2] B. B. Abelev et. al. (ALICE collaboration), Phys. Lett. B **728** (2014), 216-227 [erratum:
 98 Phys. Lett. B **734** (2014), 409-410]
 99 [3] B. B. Abelev et. al. (ALICE collaboration), Phys. Lett. B **728** (2014), 25-38
 100 [4] J. Adam et. al. (ALICE collaboration), Phys. Lett. B **758** (2016), 389-401
 101 [5] J. Adam et. al. (ALICE collaboration), Nature Phys. **13** (2017), 535-539
 102 [6] S. Acharya et. al. (ALICE collaboration), Eur. Phys. J. C **80** (2020) no.9, 889
 103 [7] S. Acharya et. al. (ALICE collaboration), Phys. Rev. C **101** (2020) no.4, 044906
 104 [8] S. Acharya et. al. (ALICE collaboration), Phys. Lett. B **800** (2020), 135043
 105 [9] S. Acharya et. al. (ALICE collaboration), Phys. Lett. B **794** (2019), 50-63
 106 [10] J. H. Chen, X. Dong, X. H. He, H. Z. Huang, F. Liu et al. arXiv:2407.02935
 107 [11] B. I. Abelev et. al. (STAR collaboration), Phys. Rev. C **75** (2007), 064901
 108 [12] B. I. Abelev et. al. (STAR collaboration), Phys. Rev. C **79** (2009), 034909
 109 [13] M. I. Abdulhamid, et. al. (STAR collaboration), Nature **632** (2024), 1026–1031
 110 [14] J. Adam et. al. (ALICE collaboration), Phys. Lett. B **754** (2016), 360-372
 111 [15] S. Acharya et. al. (ALICE collaboration), Phys. Rev. Lett. **128** (2022) no.25, 252003
 112 [16] X. Y. Ju, Y. H. Leung, S. Radhakrishnann et al., Nucl. Sci. Tech. **34** (2023) 158
 113 [17] V. Vovchenko and H. Stoecker, Comput. Phys. Commun. **244** (2019), 295-310
 114 [18] K. J. Sun, C. M. Ko and B. Dönigus, Phys. Lett. B **792** (2019), 132-137
 115 [19] D. N. Liu, C. M. Ko, Y. G. Ma, F. Mazzaschi, M. Puccio, Q. Y. Shou, K. J. Sun and
 116 Y. Z. Wang, Phys. Lett. B **855** (2024), 138855
 117 [20] J. Adam et al. (STAR Collaboration) Nature Phys. **16** (2020) 4, 409-412